Neuroimaging at 1.5 T and 3.0 T: Comparison of Oxygenation-Sensitive Magnetic Resonance Imaging

Gunnar Krüger,* Andreas Kastrup, and Gary H. Glover

Noise properties, the signal-to-noise ratio (SNR), contrast-to-noise ratio (CNR), and signal responses were compared during functional activation of the human brain at 1.5 and 3.0 T. At the higher field spiral gradient-echo (GRE) brain images revealed an average gain in SNR of 1.7 in fully relaxed and 2.2 in images with a repetition time (TR) of 1.5 sec. The tempered gain at longer TRs reflects the fact that the physiological noise depends on the signal strength and becomes a larger fraction of the total noise at 3.0 T. Activation of the primary motor and visual cortex resulted in a 36% and 44% increase of "activated pixels" at 3.0 T, which reflects a greater sensitivity for the detection of activated gray matter at the higher field. The gain in the CNR exhibited a dependency on the underlying tissue, i.e., an increase of 1.8× in regions of particular high activation-induced signal changes (presumably venous vessels) and of 2.2× in the average activated areas. These results demonstrate that 3.0 T provides a clear advantage over 1.5 T for neuroimaging of homogeneous brain tissue, although stronger physiological noise contributions, more complicated signal features in the proximity of strong susceptibility gradients, and changes in the intrinsic relaxation times may mediate the enhancement. Magn Reson Med 45:595–604, 2001.

Key words: neuroimaging; spiral scan; magnetic field strength; CNR; SNR; physiological noise

MRI modalities are often limited by the signal-to-noise ratio (SNR) and the contrast-to-noise ratio (CNR). Both SNR and CNR have been shown to increase with magnetic field strength B_0 (1,2). Consequently, the "optimal field strength" and the field dependency in blood oxygenation level dependent (BOLD) MRI have been the subject of various investigations (1,3–6). For many MRI applications a magnetic field strength of 1.5 Tesla (T) seems to represent a good compromise. Functional MRI (fMRI), however, is particularly dependent on good SNR and CNR properties, since typically observed BOLD signal changes at 1.5 T are on the order of a few percent and often exceed the intrinsic noise only slightly. Several biophysical models of activation-induced changes of the oxygenation-sensitive MRI signals have proposed that the changes in the relaxation rate ΔR_2^* and subsequently the BOLD effect are proportional to B_0 for large vessels and proportional to ${B_0}^2$ for small vessels and capillaries (7,8). Thus, higher fields may provide an important improvement in fMRI. Indeed, recent investigations have demonstrated a superlinear increase in the BOLD CNR with the field strength (1,4,5), suggesting that high field fMRI methods may be able to resolve oxygenation changes in small vessels and capillaries, which are spatially localized near the origin of the neuronal activity.

In the present study, various BOLD-relevant properties were compared at 1.5 T and 3.0 T. In order to establish identical BOLD-sensitivities, we investigated the T_2^* relaxation times for gray matter at each field strength and scaled the corresponding echo time (TE), and the excitation angle at 3.0 T. We compared intrinsic noise contributions and the SNR in gradient-echo (GRE) images and examined activation-induced BOLD responses during visual and motor activation at both fields in terms of spatial extent, the mean z-score, and the CNR of "activated voxels." T_2^*-maps from various brain sections were calculated to investigate spatial aspects and the field dependency on signal distortions in the proximity of large susceptibility gradients. Imaging parameters such as temporal and spatial resolution and sampling time (T_s) were identical for both scanners to keep SNR properties and total scan times unchanged.

THEORY

Signal-to-Noise

The SNR in high-field MR-images has been shown to be proportional to B_0 (2) and is given by:

$$\mathrm{SNR} = \omega \cdot V \cdot \sqrt{T_s} \cdot f \cdot \Psi(T_1, T_2, T_2^*), \qquad [1]$$

where ω is the operating frequency, V is the voxel size, T_s is the sampling time, $f \leq 1$ is a function that depends on the k-space trajectory in the given pulse-sequence, and Ψ is a function of various tissue parameters (T_1, T_2, T_2^*). Thus, Eq. [1] suggests that a higher field strength directly improves the SNR for a given pulse sequence. However, with higher fields T_2 and T_2^* decrease, while T_1 increases. Since T_1 increases with B_0 (~30% for 3.0 T vs. 1.5 T) the linear gain from ω with the field in GRE acquisitions with the Ernst angle (α_E) is reduced by partial saturation effects unless TR $\gg T_1$.

A recent investigation on the SNR demonstrates that the signal strength S increases with the square of the B_0-field and that the noise is proportional to B_0 (2). The total noise N in an MR image consists of at least three different noise sources (2,9):

$$\sigma = \sqrt{\underbrace{{\sigma_T}^2 + {\sigma_S}^2}_{{\sigma_0}^2} + {\sigma_P}^2}, \qquad [2]$$

where σ_T is the thermal noise, σ_S is systematic noise, σ_P physiological noise, and σ_0 is the sum of σ_T and σ_S. The physiological noise includes contributions from fluctua-

Lucas MRS Center, Department of Radiology, Stanford University, Palo Alto, CA.

Grant sponsor: Deutsche Forschungsgemeinschaft; Grant numbers: Kr 1896/1-1; Ka 1419/1-1; Grant sponsor: NIH NCRR; Grant number: RR09784.

*Correspondence to: Gunnar Krüger, Lucas MRS Center, Department of Radiology, Stanford University, Palo Alto, CA 94305.
E-mail: gkruege@s-word.stanford.edu

Received 24 June 2000; revised 1 September 2000; accepted 16 October 2000.

tions in the basal brain metabolism and thus is signal-dependent ($\sigma_P = \lambda S$). Consequently, σ_P is of increasing influence at higher fields and limits the achievable SNR at high magnetic fields. From Eq. [2], the SNR = S/σ can be written as:

$$\mathrm{SNR} = \frac{\mathrm{SNR}_0}{\sqrt{1 + \lambda^2 \cdot \mathrm{SNR}_0{}^2}}, \quad [3]$$

with $\mathrm{SNR}_0 = S/\sigma_0$ and λ a system-independent constant.

BOLD Sensitivity

Most MR neuroimaging investigations are based on long echo-time spoiled GRE acquisitions. The GRE-signal is given by:

$$S(R_1^*, R_2^*) \propto M_0 \cdot \frac{\sin(\alpha) \cdot \exp^{-TE\,R_2^*} \cdot (1 - \exp^{-TR\,R_1^*})}{1 - \cos(\alpha) \cdot \exp^{-TR\,R_1^*}}. \quad [4]$$

Thus, the measured signal in an fMRI experiment contains simultaneous inflow and BOLD effects. However, the inflow effects can be minimized by using lower flip angles and longer TRs (10–12). In the case of minimized inflow contribution ($R_1 \approx R_1^*$), the activation-induced BOLD signal change is given by:

$$\Delta S = S_0 \cdot TE \cdot \Delta R_2^* \cdot \exp^{-TE \cdot R_2^*}, \quad [5]$$

and the corresponding CNR is given by:

$$\mathrm{CNR} = \frac{\Delta S}{N} = \frac{\Delta S}{S} \cdot \frac{S}{N} = \frac{S_0}{N} \cdot TE \cdot \Delta R_2^* \cdot \exp^{-TE \cdot R_2^*}. \quad [6]$$

METHODS

Imaging and Scaling of Sequence Parameters

All experiments were conducted either at a 1.5 or 3.0 T (GE Signa Horizon, rev. 5.7, and cardiac prototype of LX, General Electric Medical Systems, Milwaukee, WI) using the standard imaging head-coil. Oxygenation-sensitive MRI acquisition was based on a GRE version of a single-shot spiral sequence (13). For this study we used a matrix size of 96 × 96 interpolated during image reconstruction to 128 × 128 over a field-of-view (FoV) of 240 × 240 mm^2. This corresponds to single-shot spiral readout windows of 40.1 ms and 39.8 ms at 1.5 T and 3.0 T, respectively. A strong signal sensitivity to changes in blood oxygenation but minimized sensitivity to inflow effects was accomplished by means of a long echo time (see below) and repetition time (TR = 1.5 sec in activation protocols). Image reconstruction was performed offline using a gridding algorithm (14). Retrospective first-order shim correction was performed using a B_0-field map calculated for each slice from the first two frames with different echo-times (ΔTE = 2 ms) resulting in an average root mean square (RMS) of 5.9 and 8.1 Hz over the head area at 1.5 T and 3.0 T, respectively. In order to keep BOLD-sensitivity and susceptibility effects in GRE-imaging at the higher field unchanged, we scaled TE and the flip angle with respect to T_1 and T_2^* properties at 1.5 T and 3.0 T (15–17). In initial experiments we determined relevant T_2^*-relaxation times of gray and white matter brain tissue at each field by means of a modified pulse sequence. During 100 single-shot acquisitions (TR = 3.0 sec), the actual TE was increased by 2 ms with every concomitant repetition resulting in 100 images with a range of TEs between 5 ms and 203 ms. We calculated pixel-wise T_2^*-maps and the corresponding χ^2-maps by fitting the signal intensities time courses to a mono-exponential decay. Larger χ^2-values indicate a divergence from the mono-exponential decay, and thus this metric is sensitive to signal losses near susceptibility gradients. In order to compute gray and white matter T_2^* values we used images from the T_2^* mapping sequences to segment the gray and white matter areas. The computed T_2^* relaxation times for gray and white matter present the average value from the corresponding segmented cortical matter in the calculated T_2^*-maps. Based on computed transverse relaxation times in cortical gray matter of T_2^* = 65 ms and 49 ms at 1.5 T and 3.0 T, respectively, we used TE = 40 ms for imaging at 1.5 T, and TE = 30.0 ms at 3.0 T. To further maximize the BOLD effect (1,12) but minimize possible inflow effects we used only a fraction (0.9-fold) of the Ernst angle (α_E). According to the differences in T_1-relaxation times in gray matter at different field strength (15–18), we used $\alpha_E = 67°$ at 1.5 T and $\alpha_E = 64°$ at 3.0 T, respectively.

Signal-to-Noise and Physiological Noise

SNR in T_2^*-weighted images was determined by averaging separately the even and odd numbered frames from the 40 initial baseline images in the fMRI trials. Subsequently, sum and difference images were obtained by adding and subtracting the two average images. The SNR was calculated as the ratio of the mean value (signal) from a brain region in the sum image and the standard deviation (noise) in the same ROI in the difference image. A more detailed discussion of this method to calculate SNR has been published recently (19). Note that the SNR calculation was based on an ROI encompassing a mixture between white and gray matter and covering major parts of the brain in the section.

In a separate set of experiments we measured the contribution of the B_0-dependent noise σ_0 and the physiological noise σ_P to the total image noise σ. Since the physiological noise depends on the signal strength itself (Eq. [2]) modulations of the flip angle were used to vary the signal and thus the fraction of physiological noise to the total noise. Therefore, we acquired sequences of oxygenation-sensitive MR images with TR = 3.0 sec and TR = 5.4 sec (fully relaxed) from the resting brain with different excitation angles between 1° and 90°. At 1.5 T 10 subjects and at 3.0 T 11 subjects (age 26–40 years, 30 ± 4 years) were scanned with either protocol consisting of six 5.5-min trials (TR = 3000 ms, 100 frames, 3 slices, 15°, 30°, 45°, 60°, 75°, and 90°) or (TR = 5400 ms, 60 frames, 3 slices, 1°, 12°, 24°, 37°, 53°, and 90°).

Functional Neuroimaging

A total of seven healthy subjects (age 25–36 years, 29 ± 4 years) participated in functional neuroimaging experi-

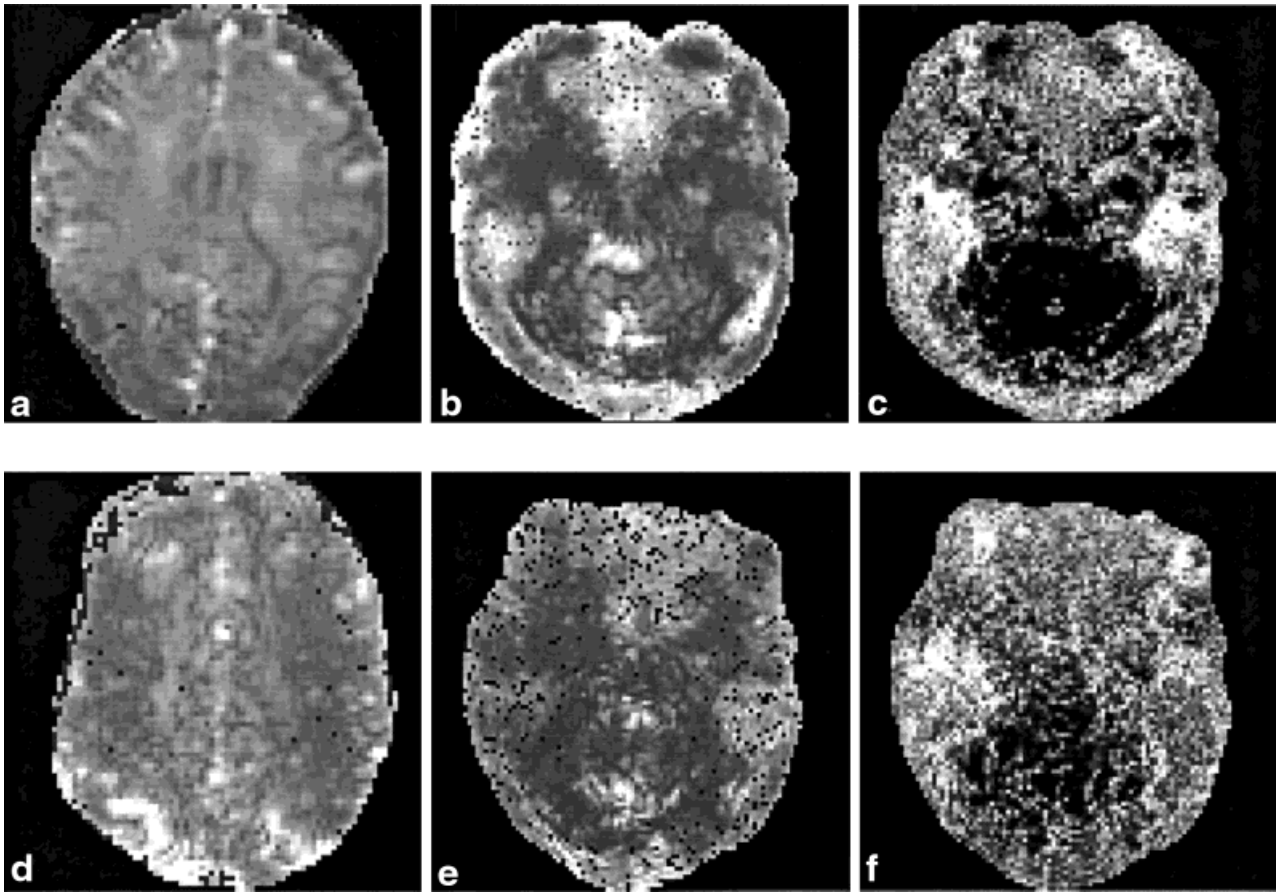

FIG. 1. Typical T_2^*-maps from an oblique brain section covering major parts of the calcarine fissure at 1.5 T (**a**) and a section parallel to AC-PC covering parts of the motor cortex at 3.0 T (**d**). The remaining pictures demonstrate T_2^*-maps and the corresponding χ^2-maps from one subject and similar brain section at 1.5 T (**b, c**) and at 3.0 T (**e, f**). The χ^2 map at 1.5 T (**c**) exhibits small (black) variations from the exponential signal decay in the posterior brain area, but strong variations (light) from the expected exponential decay in the areas of air–tissue interfaces near the ear–air-holes. The corresponding map from an almost identical imaging section at 3.0 T (**f**) shows a more extended region of affected brain tissue in the proximity of the air–tissue interfaces.

ments with visual and motor stimulation on each scanner. One subject was scanned twice. Conventional T_1-weighted GRE images (TR/TE/flip = 70/5/60°) were obtained for anatomic reference. For visual activation protocols we encompassed major parts of the calcarine fissure by means of three oblique slices (4 mm slice thickness, 0.5 mm gap). During motor tasks we acquired five slices (4 mm slice thickness, 0.0 mm gap) parallel to the AC-PC line. These sections covered most parts of the sulcus precentralis, centralis, and postcentralis as well as the SMA. The repositioning of each volunteer in the second session (other field strength) was based on scout images from the first session. On both scanners we used the same video projection setup (Resonance Technology, Van Nuys, CA) for visual activation. The visual stimulation paradigm was based on sequences of computer-generated images transferred directly to the projection system and involved presentations of a black–white checkerboard paradigm reversing at a frequency of 5 Hz. The control condition was a black screen with a small fixation cross. Subjects were instructed to keep their eyes open, pay constant attention during the individual experiments, and to fixate on the centered cross. Motor stimulation was accomplished by an auditorily paced bilateral finger-tapping task with a frequency of 3 Hz involving all fingers.

In each session two visual and two motor activation protocols with identical timing were performed. The protocol consisted of five repetitive cycles with alternations between 18 sec stimulation and 36 sec control condition. In order to calculate the prestimulus baseline intensities an initial control phase of 60 sec preceded the activation cycles. Moreover, the final control period was also expanded to 60 sec to monitor the return to the prestimulus baseline.

Activation was determined by a pixel-wise calculation of the *z*-score associated with the signal intensity time courses and a boxcar reference waveform (10). The reference function represented the applied stimulation protocol shifted by three images with respect to onset of activation to account for hemodynamic latencies. The first two images were discarded to eliminate saturation effects. Quantitative maps of *z*-scores were analyzed, thresholded (99.99% significance level), and color-coded as described previously (11). A red-yellow color table was scaled to the range between the cutoff-threshold and the highest *z*-score in the individual activation maps. To further minimize

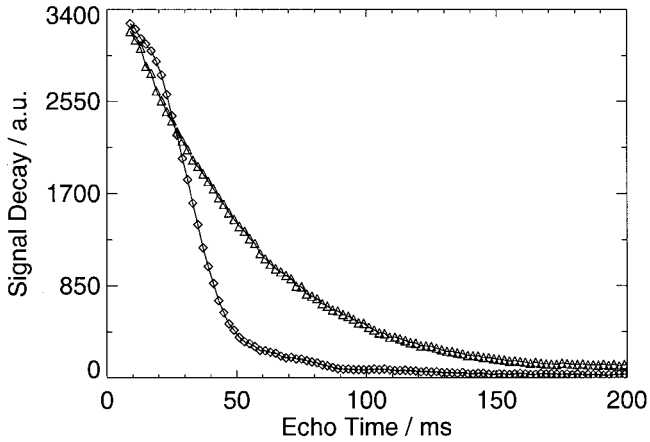

FIG. 2. Signal decay in gradient-echo MRI as a function of echo time in a homogeneous brain ROI (triangle) and in the proximity of susceptibility gradients from air–tissue interfaces (diamond) at 3.0 T.

false–positive admitted pixels, we calculated maps of standard deviation and excluded pixels with high standard deviation, i.e., pixels outside the brain section and at the brain surface, from the analysis. Neither temporal nor spatial filters were applied. Regional signal intensity time courses were derived as the mean of all activated pixels admitted by the analysis.

Motivated by the fact that temporal BOLD responses from the foci within a cluster of activated areas, i.e., pixels demonstrating the highest statistical significance, exhibit greater signal changes than the average responses from the overall activated areas, we examined the CNR according to Eq. [6] as a function of the number of activated pixels. The corresponding mean BOLD signal changes were computed from 10–220 statistically significant activated pixels. The calculated CNR with respect to different sizes of activated gray matter represent the average temporal response from pixels with the highest z-score at a time.

RESULTS

T_2^*-Relaxation Times, BOLD Signals, and Sensitivity

Figure 1a–c (top row) demonstrate a T_2^*-map from a typical brain section for a visual activation experiment (Fig. 1a), as well as a T_2^*-map (Fig. 1b) and the corresponding χ^2-map (Fig. 1c) from an imaging section with strong susceptibility gradients in the proximity of air–tissue interfaces at 1.5 T. Figure 1d shows a T_2^*-map at 3.0 T from a typical brain section for a motor experiment parallel to AC-PC. Figure 1e, f demonstrate T_2^*- and χ^2-maps at 3.0 T from the same subject and very similar brain sections as in Fig. 1b, c. In the homogeneous cortical gray and white matter we found mean T_2^* relaxation times of 65 ms and 78 ms at 1.5 T, respectively. At the higher field both gray and white matter exhibited mean T_2^* relaxation times of 49 ms. The T_2^*-maps and in particular the χ^2-maps highlight a fundamental problem of long-TE GRE imaging at higher fields. Susceptibility gradients at air–tissue interfaces, as visible in the selected slice (Fig. 1b–c and 1e–f), influence the homogeneity in neighbor tissue. The affected brain regions as indicated by a large χ^2-value (bright gray values) spread out with the higher field and suffer from stronger intravoxel dephasing or even a total signal loss in long-TE images. In order to demonstrate that phenomenon we plot the GRE signal decay in different ROIs as a function of TE (see Fig. 2). Whereas the signals from a small ROI (182 pixels) in an homogeneous brain area exhibit an exponential decay (triangle symbols in Fig. 2) the corresponding signals from an ROI (168 pixels) in the proximity of susceptibility gradients demonstrate a more complicated signal behavior (diamond symbols in Fig. 2), characterized by an early strong signal decay (data shown here are from 3.0 T). However, signal decays from homogeneous brain areas such as the visual and motor cortices usually show a mono-exponential functionality. Plots of the corresponding BOLD sensitivity according to Eq. [6] from a representative homogeneous gray matter compartment and both fields in one subject are shown in Fig. 3. The signal maximum indicates the maximum BOLD sensitivity and concurrently the T_2^*-relaxation time.

Spatial Extent of Activation

Figure 4 demonstrates activation maps from a reversing checkerboard paradigm at 1.5 T (Fig. 4a–c) and at 3.0 T (Fig. 4d–f), as well as from the paced finger-tapping task at 1.5 T (Fig. 4g–i) and 3.0 T (Fig. 4j–l). All maps are from one subject and very similar sections. The two paradigms elicited similar activations in terms of the center (foci) of activation at each field strength, but resulted consistently in a higher sensitivity for the detection of activated areas at the higher field. An intersubject analysis revealed 222 ± 71 (1.5 T) and 319 ± 122 (3.0 T) activated image pixels in the sections covering the visual cortex, and 165 ± 33 (1.5 T) and 225 ± 34 (3.0 T) activated image pixels in

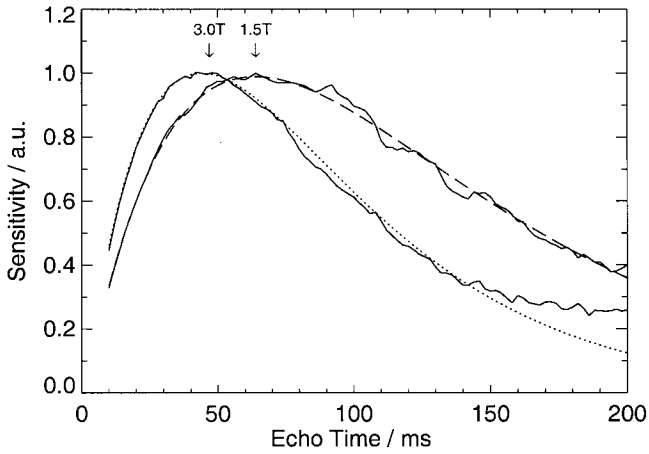

FIG. 3. Signal decay in a homogeneous brain region multiplied by the TE as a function of the echo time from one subject at 1.5 T and 3.0 T. The maximum of the graphs present the highest BOLD-sensitivity at each field. The solid lines represents the experimental data. The broken line shows the best fit on the signal decay at 3.0 T. The dotted line demonstrates the corresponding signal responses at 1.5 T. Note that the maximum of the graph also denotes the T_2^* relaxation time at each field strength. The arrows indicate the average T_2^*-relaxation times at 1.5 T and 3.0 T, respectively.

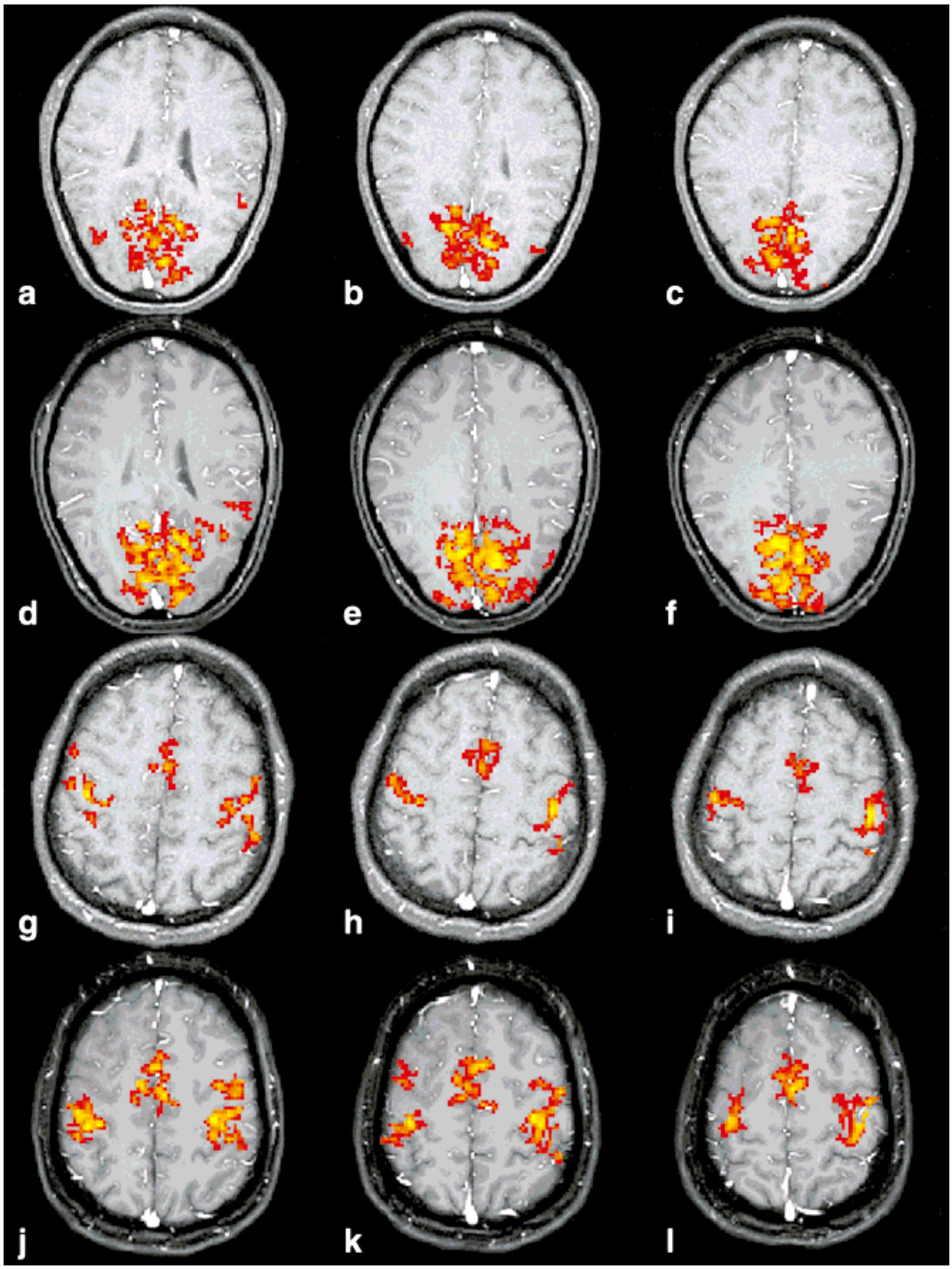

FIG. 4. Spatial extent of activated cortical gray matter from a repetitive checkerboard activation at 1.5 T (**a**–**c**) and at 3.0 T (**d**–**f**), as well as the corresponding responses from activation of the motor cortex at 1.5 T (**g**–**i**) and 3.0 T (**j**–**l**). All activation maps are from same subject and very similar imaging sections. Shown are three contiguous slices from the visual and motor protocol.

the corresponding sections covering the motor cortex (values from all subjects are listed in Table 1). Thus, in cortical areas of the visual and motor system we found a 44% and 36% increase in activated pixels at 3.0 T, respectively. Moreover, the mean *z*-score in activated areas was 1.7-fold (visual cortex) and 1.9-fold (motor cortex) higher at 3.0 T, also visible in Fig. 4, as more color-coded pixels demonstrate bright yellow colors.

Temporal Aspects

Intersubject averages of regional time courses for repetitive activation protocols are summarized in Fig. 5. The temporal responses refer to a reversing checkerboard paradigm at 1.5 T (Fig. 5a) and at 3.0 T (Fig. 5b), as well as to the paced finger-tapping task at 1.5 T (Fig. 5c) and at 3.0 T (Fig. 5d). The activation-induced positive signal response in the vi-

Table 1
Number of Activated Brain Voxels (1.9 mm × 1.9 mm × 4.0 mm Voxel Size) From All Seven Subjects

Subject	1.5 T (V1)	3.0 T (V1)	1.5 T (M1)	3.0 T (M1)
1	138 ± 15	235 ± 90	135 ± 34	210 ± 63
2	295 ± 20	400 ± 29	229 ± 31	248 ± 35
3	184 ± 44	250 ± 57	156 ± 15	207 ± 41
4	328 ± 20	521 ± 65	163 ± 25	262 ± 72
5	176 ± 27	152 ± 13	152 ± 20	173 ± 38
6	179 ± 65	307 ± 28	—	—
7	255 ± 80	365 ± 75	152 ± 30	250 ± 80
Mean	222 ± 71	319 ± 122	165 ± 33	225 ± 31

Values from the visual and motor protocols are listed separately. Subject 6 was exempted from the motor task due to inability to keep the task frequency of 3 Hz.

sual protocol exhibited signal changes of 2.8% (1.5 T) and 2.9% (3.0 T). The negative poststimulus response resulted in −0.6% (1.5 T) and −0.8% (3.0 T), respectively. The corresponding signal changes during the motor task demonstrated 2.2% for the positive response at both 1.5 T and 3.0 T, but only a mild negative poststimulus response of −0.1% (1.5 T) and −0.3% (3.0 T).

Signal-to-Noise and Image Noise

The SNR in GRE images was consistently greater at the higher field. The SNR as a function of the SNR_0 ($SNR_0 = S/\sigma_0$) at excitation angles of 1°, 12°, 24°, 37°, 53°, and 90° in fully relaxed (TR = 5400 ms) GRE images in resting brain is shown in Fig. 6. Data from 1.5 T and 3.0 T are plotted with square and triangle symbols, respectively. At 3.0 T, the physiological noise is of increasing influence at higher excitation flip angles (larger signals) and results in the divergence of the SNR-to-SNR_0 ratio from the line-of-identity (dotted line). In quasi-fully relaxed images (TR = 5.4 sec) the physiological noise clearly affects the gain in SNR for greater flip angles (≥37°). Extrapolations to a signal strength $S = 0$ (using Eq. [2]) exhibited a 1.6× increase of σ_0 at 3.0 T. The computation of the corresponding gain in SNR showed an average increase of 1.7 at the higher field. Similar experiments with a repetition time of TR = 3.0 sec demonstrated a gain in SNR of ~1.8. Besides

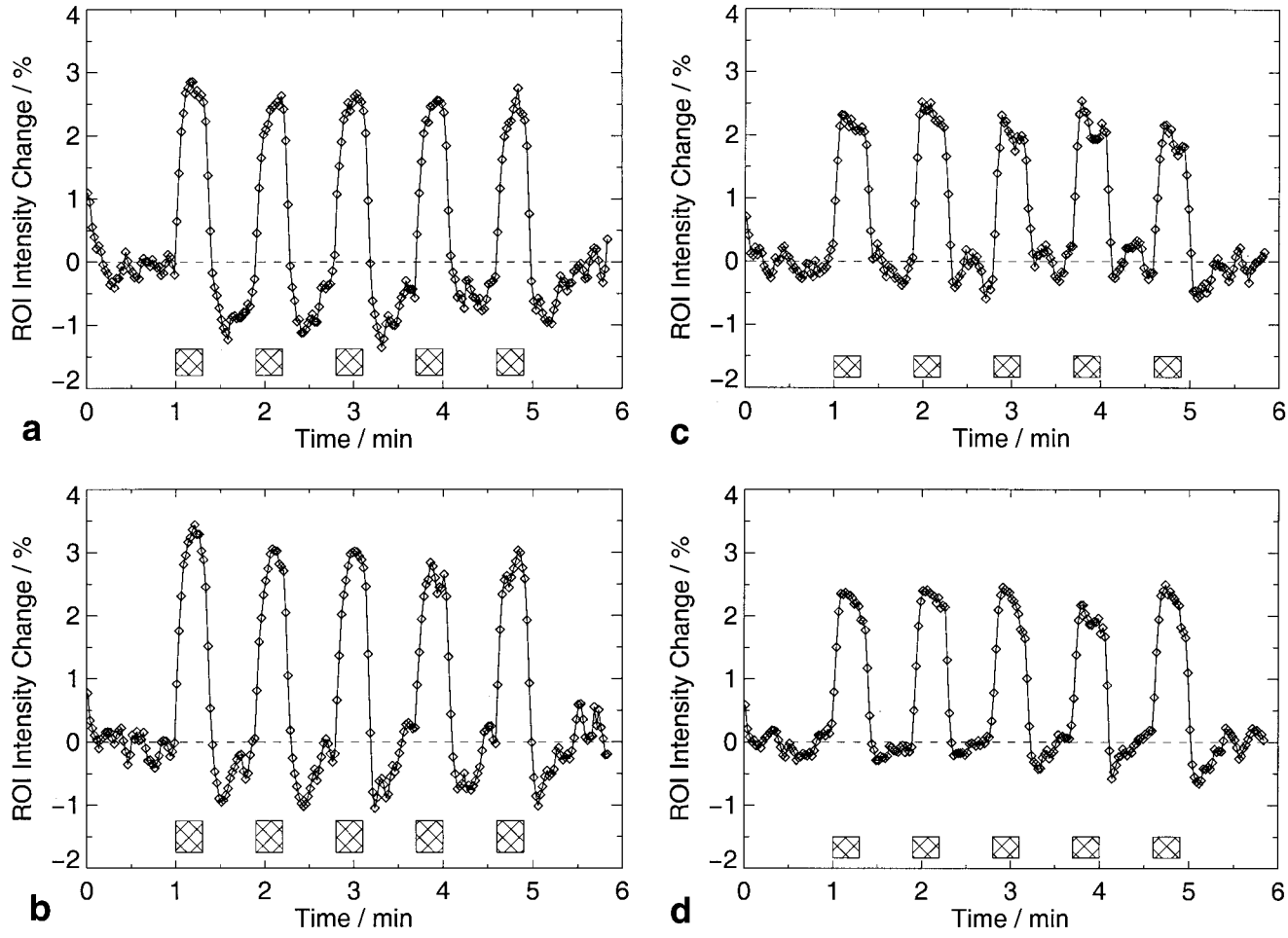

FIG. 5. Normalized regional average time courses of oxygenation-sensitive MRI signal intensities for the repetitive visual (n = 7) and motor stimulation (n = 6) vs. control. The temporal responses (TR = 1.5 sec) exhibited an average standard error of the mean of 0.25% ± 0.05% (error bars not shown) and refer to (**a**) 5 Hz reversing checkerboard at 1.5 T, (**b**) 5 Hz checkerboard at 3.0 T, (**c**) 3 Hz finger-tapping at 1.5 T, and (**d**) the same motor task at 3.0 T. Horizontal dashed lines indicate the mean prestimulus baseline and crosshatched bars indicate periods of activation. Note that responses from an individual subject represent the mean response from three slices and two trials.

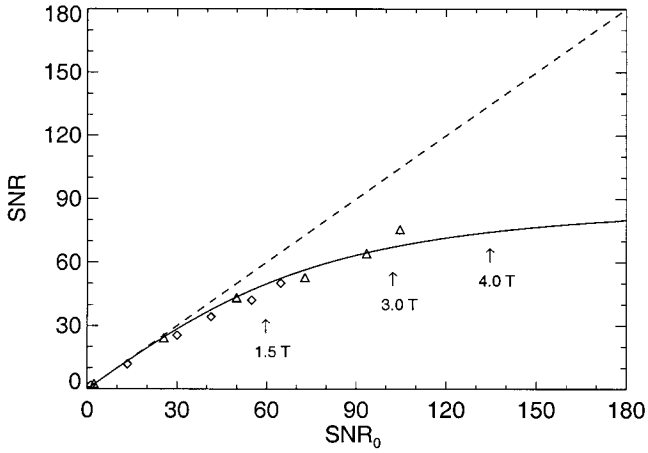

FIG. 6. The SNR as a function of SNR_0 in fully-relaxed GRE images (TR = 5.4 sec). Data represent ratios from excitation flip angles of 1°, 12°, 24°, 37°, 53°, 90° at 1.5 T (square, n = 5) and 3.0 T (triangle, n = 6). The dotted line demonstrates the line-of-identity. The arrows indicate points on the curve for the flip angles used in the neuroimaging experiments and predict the corresponding point for 4.0 T if similar coil and system noise were used.

these experiments, the SNR calculation from the baseline images in the functional trials (TR = 1.5 ms) showed an average gain of 2.2. The corresponding SNR values are listed in Table 2.

Contrast-to-Noise

Figure 7a demonstrates the dependency of the average percentage signal change in activated cortical gray matter as a function of the number of underlying activated pixels having the highest *z*-scores in the activation maps. It was found that, apart from contributions from vessels, which are characterized by greater noise levels, the highest statistical significance usually matches the voxels with the greatest BOLD response. The corresponding gain in CNR ($CNR_{3.0\ T}/CNR_{1.5\ T}$) from signal responses in activated brain areas between 10 and 220 pixels (141–3094 mm^3) is shown in Fig. 7b. The gain ranges between 1.8 with only 10 activated pixels and 2.2 with 220 activated pixels and demonstrates an overall steady increase with the size of activated brain tissue. The graph is an average response from the visual protocol from three subjects, who showed in all three slices and all experiments a minimum of 220 activated pixels. Similar results were obtained from the motor activation.

Table 2
SNR in GRE Images Computed From the Initial 40 Baseline Images in the fMRI Trials

Subject	1.5 T (V1)	3.0 T (V1)	1.5 T (M1)	3.0 T (M1)
1	23.5	94.4	25.1	82.5
2	32.2	69.4	32.2	58.2
3	33.1	93.4	33.3	93.5
4	35.7	63.9	34.9	77.9
5	33.7	90.3	47.7	91.8
6	43.1	76.8	59.5	86.9
7	42.3	85.2	46.0	81.2
Mean	34.8 ± 6.6	81.9 ± 12.1	39.8 ± 11.8	81.7 ± 11.8
Gain		2.35		2.05

SNRs from imaging sections for the visual and motor protocol are listed separately. In all seven subjects the SNR was consistently higher at 3.0 T.

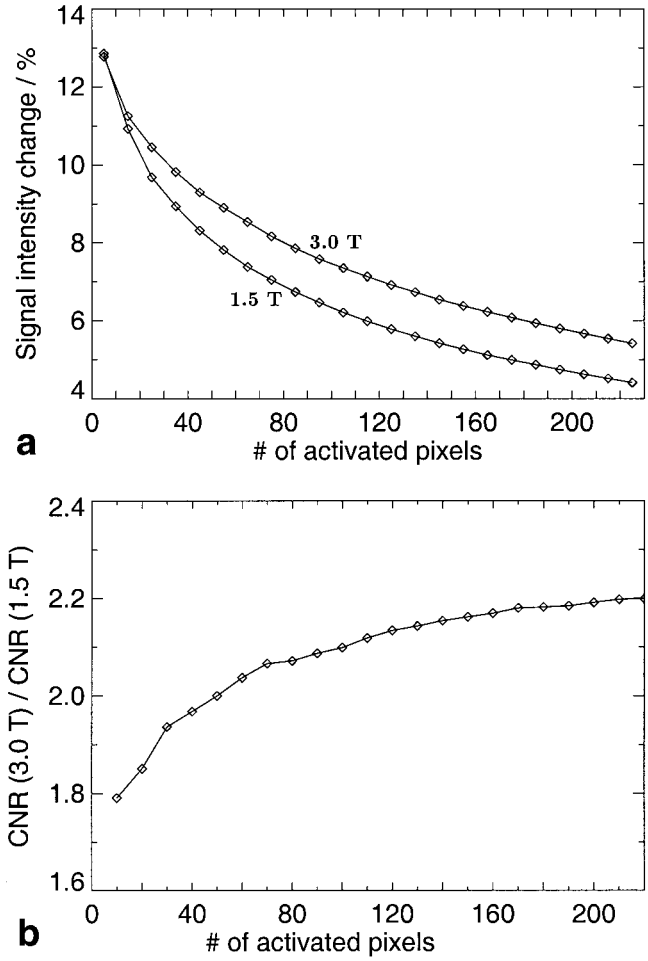

FIG. 7. The dependence of the average percentage signal change on the number of activated pixels during visual activation (**a**). The admitted activated pixels demonstrate the mean responses from the pixels with the highest *z*-score at a time (n = 3). The signal change in small restricted activated areas is similar at both fields, but diverges with larger numbers of activated brain pixels. The ratio of CNR at 3.0 T and CNR at 1.5 T as a function of the size of activated brain area is shown in **b**. Although the number of activated areas is much smaller in the motor protocol, we found very similar properties (data not shown).

DISCUSSION

Intrinsic Tissue Parameters

The measured T_2^* times of 65 ms (1.5 T) and 49 ms (3.0 T) in gray matter and 76 ms (1.5 T) and 49 ms (3.0 T) in white matter of the human brain are in good agreement with recently published data (1,17). In particular, a recent investigation at 3.0 T (17) has reported T_2^* values of 44.7 and 48.4 ms for occipital and frontal white matter, respectively, as well as 41.6 and 51.8 in occipital and frontal gray matter. Our values present average T_2^* across the brain and

thus match the average T_2^* values in (17). Interestingly, the computation of the T_2^* in the regions of the occipital lobe, which elicited significant signal changes upon activation, resulted in a T_2^* value of 44 ms, in line with the report of shorter T_2^* values in the occipital lobe (17).

SNR

The observation of a gain in the SNR by 2.2 at 3.0 T in typical GRE-MRI (TR = 1.5 sec) is in good agreement with the expected linear relationship between the SNR and the field strength and the computed gain in SNR between 1.7 (TR = 5.4 sec) and 1.8 (TR = 3.0 sec) for long TR images. The differences in the SNR gains may be attributed to saturation effects at shorter TRs. Saturation effects lead to a reduced signal strength and thus influence the degree of the signal dependent physiological noise on the total image noise. Note that, although the gain in SNR at 3.0 T increases at shorter TRs, the relevant absolute SNR in the MRIs decreases in the presence of saturation effects. The signal strength and the fraction of physiological noise on the total image noise can also be varied by the excitation flip angle. Thus, specific care has to be taken during the design of imaging experiments, as an improper choice of sequence parameter can easily diminish the promised gain in SNR. Notably, the T_1 relaxation time in brain tissue increases with field strength (15,17,18,20) and thus counteracts the gain from ω in SNR and CNR in GRE sequences with TR $\ll T_1$ at higher fields (see Theory). Beyond that, we employed very similar sampling times at both fields (T_s = 40.1 ms and T_s = 39.8 ms). At higher fields the shorter T_2^* relaxation time results in an increased broadening of the point-spread-function (19,21), causing more blurring in spiral imaging and distortions in conventional echo-planar imaging (EPI). Additionally, field inhomogeneities scale with B_0 and cause not only further off-resonance blurring but also stronger signal losses in regions affected by magnetic field susceptibilities. Thus, a sampling time on the order of the intrinsic T_2^* relaxation time reduces the SNR and the CNR and is a particularly critical parameter in single-shot imaging methods.

Physiological Noise

The measured SNR in fully relaxed MRIs exhibits a supralinear increase with signal strength, as shown in Fig. 6. This arises because of the increasing contribution of the physiological noise to the total image noise (Eq. [2]), which depresses the gain since σ_P is proportional to the signal. Note that a single curve with $\lambda = 0.011$ fits both 1.5 and 3.0 T data, which suggests that the model in Eq. [3] is reasonable. At the reduced flip angles employed in the functional experiments here, the fractional SNR losses at 1.5 and 3.0 T were 0.83 and 0.66, respectively, corresponding to the arrows in Fig. 6. This amounted to fractional contributions in physiological noise σ_P/σ_0 of 0.67 at 1.5 T and 1.14 at 3.0 T. If the model (Eq. [3]) holds at higher fields and assuming the same coil efficiency so that SNR_0 is linear with B_0, an interpolation predicts that $\sigma_P/\sigma_0 \approx 1.5$ at 4.0 T. These results strongly suggest that at higher fields the true gain in SNR in a BOLD experiment is substantially reduced from that expected with thermal limits alone. A separate computation of λ's from 1.5 T ($\lambda_{1.5\,T}$ = 0.0156) and 3.0 T ($\lambda_{3.0\,T}$ = 0.0108) exhibited a slight difference between the two fields. Since phantom data also demonstrated a weak divergence from SNR_0 at high SNRs ($\lambda_{1.5\,T} \leq 0.0042$) and ($\lambda_{3.0\,T}$ = 0.0024), we believe that these small differences reflect the individual noise properties of each system. Furthermore, λ's from small gray and white matter ROIs also demonstrated differences, in agreement with an earlier study on the noise in fMRI data (9).

CNR

The present comparison of BOLD CNR at 1.5 T and 3.0 T demonstrates that, besides the benefit of the higher field, the CNR is dependent on the underlying tissue and vascular structure. Theoretically, ΔR_2^* has been proposed to be proportional to ${B_0}^p$ with $p \approx 1$ for contribution from larger vessels and $p \approx 2$ for smaller vessels and tissue (7). The expected gain at 3.0 T in the CNR can be estimated according to Eqs. [5] and [6] using the imaging parameters (TR = 1.5 sec, $TE_{1.5\,T}$ = 40 ms, $TE_{3.0\,T}$ = 30 ms, $\alpha_{1.5\,T} = 67°$, $\alpha_{3.0\,T} = 64°$), and typical parameters for brain relaxation times $T_{1_{1.5\,T}}$ = 1.0 s (15), $T_{1_{3.0\,T}}$ = 1.33 s (17), $\Delta R^*_{2v_{1.5\,T}} = -3.06\ s^{-1}$, $\Delta R^*_{2t_{1.5\,T}} = -0.32\ s^{-1}$ (1), $\Delta R^*_{2v_{3.0\,T}} = -4.4\ s^{-1}$, $\Delta R^*_{2t_{3.0\,T}} = -0.8\ s^{-1}$ (tissue and vessel R_2^* values for 3.0 T interpolated from 1.5 T and 4.0 T in (1)), as well as $T^*_{2_{1.5\,T}}$ = 65 ms, and $T^*_{2_{3.0\,T}}$ = 49 ms (see Results). Assuming that S_0/N demonstrates a linear dependency on the magnetic field strength, the expected gain in CNR ranges between 2.0–3.4 for vessels and tissue contributions, respectively. We observed increases in the CNR between 1.8 for the foci of activation (≈10 pixels) and 2.2 for larger areas of activated brain regions (>100 pixels). The CNR derived from extremely small activated areas (10–50 pixels) most likely reflects the contribution from primarily large vessels (22), as the corresponding BOLD signals showed the highest percentage signal changes (Fig. 7a). This is supported by a recent investigation (23), which clearly demonstrates that the average percentage signal change in activated areas is a function of the "cutoff" threshold and thus a function of the admitted activated pixels. Notably, high percentage signal changes are further emphasized by the high spatial resolution of $1.9 \times 1.9 \times 4\ mm^3$. The corresponding CNR from larger areas of activated brain regions (>100 pixel) presumably represent a mixture between signals from rather coarse vessel structures and brain tissue, i.e., capillaries and small venules. Thus, the observed gain in CNR at the higher field can be considered to be in good agreement with theoretical predictions (7) as well as with recent investigations (1,5). However, further increases in the spatial resolution and suppression of inflow effects may lead to an increased gain in CNR at the higher field.

In contrast to an earlier investigation that reported large increases in BOLD-signal changes ($\Delta S/S$) of up to 28% upon activation at 4 T, but rather small maximum changes of 7% at 1.5 T (4), we observed only small differences in the mean BOLD signal change at each field strength. The maximum observed signal changes in small areas of 10 activated pixels was found to be 17% at 1.5 T and 15% at 3.0 T. In the present investigation we used a TE of only 0.6-fold of the corresponding TE with the highest BOLD sensitivity, e.g., TE = 40 ms instead of 65 ms at 1.5 T.

Thus, it can be assumed that the overall BOLD signal change exhibits a weaker sensitivity than the hypothetical BOLD signal variation at a highest sensitivity. However, this consideration can only explain the differences between the observation of BOLD signal changes at 3.0 T (present study) and, e.g., 4.0 T. The most likely explanation of a 4-fold increase in the MR signal variation at 1.5 T and 4.0 T is that the authors (4) used surface coils with different spatial sensitivities. According to Eq. [5] we expect an increase in the relative BOLD signal changes ($\Delta S/S$) of 1.1 in vessel voxel and 1.9 in tissue voxel (ΔR_2^* from [1] and neglect inflow effects). Note that the scaling of TE counterbalances the greater ΔR_2^* at higher fields. Again, hypothesizing that small regions of highly significant activated areas represent vessels rather than tissue voxel, the finding of very similar BOLD signal variations at both fields (Fig. 7a) is in excellent agreement with the theoretical predictions.

Spatial Aspects of Activated Brain

During both motor and visual activation we observed a steady increase in the number of activated pixels. We tacitly assume human cognitive processes are unaffected by the magnetic field. Therefore, the observation of an increased number of activated pixels (36% and 44%) corresponds to an improved CNR and concomitantly more accurate statistics. This is supported by the finding of a gain in the CNR > 2 in the average activated brain voxel at the higher field. In addition, the finding of a 1.8-fold increase in the mean *z*-score in activated brain areas corresponds to the improved CNR and the higher accuracy in the statistical procedure. The findings of a greater number of activated pixels and an overall increase in the *z*-score are in line with a recent investigation (5), reporting a 70% greater number of activated pixels and a 20% higher average *t*-score. Although the present results from 3.0 T are not directly comparable with the investigation at 4.0 T (5), we expect a further increase of the CNR in homogeneous brain areas at 4.0 T, which would lead to an improved statistical accuracy.

It can be argued that the similar sampling durations of $T_s = 40.1$ ms (1.5 T) and $T_s = 39.8$ ms (3.0 T) result in a better point spread function at the lower field due to the reduced T_2^* at 3.0 T. The corresponding loss in spatial specificity to the center of neuronal activity at the higher field could thereby explain the detection of an increased number of activated voxels. However, the RMS field homogeneity after the slice-by-slice shim correction was typically 5.9 Hz and 8.1 Hz over the head area at 1.5 T and 3.0 T, respectively, both of which values are well below that required for significant blurring and affection of the point spread function (19).

Temporal Aspects of Activated Brain

The temporal response pattern from activated gray matter were very similar at each field strength for both activation of the visual and the motor cortex. Interestingly, the responses from checkerboard activation exhibited a pronounced undershoot phenomenon and an apparent baseline drift due to the short interstimulus interval and an incomplete signal recovery (24), not clearly visible in the responses from activation of the motor cortex (23,25). Also, the peak-to-peak responses from the finger-tapping task are significantly smaller than the visual responses. Recent investigations have demonstrated that the post-stimulus undershoot is primarily a delayed blood volume and/or metabolic regulation (26,27). Earlier studies have shown that the BOLD signal changes in the venous vessel are more coarse than in the tissue contributions (22). Thus, the smaller BOLD signal change in the motor responses as well as the weak undershoot phenomenon may be explained by the fact that the MRI responses in motor areas rather represent contributions from tissue and small vessels.

Susceptibility Gradients

The present findings of enhancements in SNR, CNR, and statistical accuracy in fMRI at the higher field are based on neuroimaging in comparatively homogeneous brain regions such as the primary visual and motor cortex. The demonstrated good agreement between experimental and theoretical determination of SNR and CNR issues relies on the mono-exponential signal decay with T_2^*. In contrast to homogeneous brain tissue, this fundamental signal behavior is perturbed in regions of strong susceptibility gradients, e.g., near air–tissue interfaces (see Fig. 2). An imposed field gradient (ΔB) scales with B_0 and results in a more complex signal decay, also demonstrated by the increased variation in the χ^2-maps at 3.0 T (compare Fig. 1e, f). Thus, GRE neuroimaging methods which focus on affected brain areas may suffer from strong signal perturbations caused by existing intrinsic magnetic field gradients. Although higher spatial resolution can partially solve the problem, field inhomogeneities can lead in the worst case to a complete MR signal dropout.

CONCLUSIONS

In agreement with recent investigations (1,4,5), the present results demonstrate a gain in SNR and CNR in homogeneous brain areas at a higher magnetic field strength. In fully relaxed MRI experiments at 1.5 T the fraction of the physiological noise σ_P to the noise contribution σ_0 was found to be 0.65. The corresponding proportion at 3.0 T demonstrated a substantial increase to 1.12× of σ_0. However, the influence of σ_P on the SNR in non-fully relaxed MRIs (TR = 1.5 sec) with reduced flip angles ($\alpha = 67°/64°$) was found to be modest. More importantly, the present results strongly suggest that neuroimaging at magnetic fields beyond 4.0 T clearly suffer from the increasing influence of physiological noise in such a way that only moderate further gains in SNR and CNR can be expected. Activated pixels were found to be significantly more extensive at the higher field (36% and 44%) and the mean *z*-score in activated pixel was 1.8-fold higher. However, in order to realize the promised improvement in SNR and CNR, various counteracting factors, such as changes of T_1- and T_2^*-relaxation times, as well as higher requirements in technical precision, e.g., gradient system and RF-coil efficiency at the higher field, have to be taken into account. Also, the reported gains at higher fields are tempered in

regions near air–tissue interfaces by greater susceptibility losses. Nevertheless, the fundamental gains in many regions of the brain provide strong impetus for the use of higher B_0-fields in fMRI.

ACKNOWLEDGMENTS

The authors thank A.M. Sawyer-Glover for assistance and T.J. Brosnan for technical support.

REFERENCES

1. Gati JS, Menon RS, Ugurbil K, Rutt BK. Experimental determination of the bold field strength dependence in vessels and tissue. Magn Reson Med 1997;38:296–302.
2. Edelstein WA, Glover GH, Hardy CJ, Redington RW. The intrinsic signal-to-noise ratio in nmr imaging. Magn Reson Med 1986;3:604–618.
3. Hoult DI, Chen CN, Sank VJ. The field dependence of NMR imaging: II. Arguments concerning an optimal field strength. Magn Reson Med 1986;3:730–746.
4. Turner R, Jezzard P, Wen H, Kwong KK, Le Bihan D, Zeffiro T, Balaban RS. Functional mapping of the human visual cortex at 4 and 1.5 Tesla using deoxygenation contrast epi. Magn Reson Med 1993;29:277–279.
5. Yang Y, Wen H, Mattay VS, Balaban RS, Frank JA, Duyn JH. Comparison of 3D bold functional MRI with spiral acquisition at 1.5 T and 4.0 T. NeuroImage 1999;9:446–451.
6. Cohen MS, Bookheimer SY. Localization of brain function using magnetic resonance imaging. Trends Neuro Sci 1994;17:268–277.
7. Ogawa S, Menon RS, Tank DW, Kim SG, Merkle H, Ellermann JM, Ugurbil K. Functional brain mapping by blood oxygenation level-dependent contrast magnetic resonance imaging. A comparison of signal characteristics with a biophysical model. Biophys J 1993;64:803–812.
8. Fisel CR, Ackerman JL, Buxton RB, Garrido L, Belliveau JW, Rosen BR, Brady TJ. MR contrast due to microscopically heterogeneous magnetic susceptibility: numerical simulations and applications to cerebral physiology. Magn Reson Med 1991;17:336–347.
9. Weisskoff RM, Baker J, Belliveau J, Davis TL, Kwong KK, Cohen MS, Rosen BR. Power spectrum analysis of functionally-weighted MR data: what's in the noise? Proc ISMRM 1993;1:7.
10. Frahm J, Merboldt KD, Hänicke W, Kleinschmidt A, Böcker H. Brain or vein—oxygenation or flow? On signal physiology in functional MRI of human brain activation. NMR Biomed 1994;7:45–53.
11. Duyn JH, Moonen CT, van Yperen GH, de Boer RW, Luyton PR. Inflow versus deoxyhemoglobin effects in bold functional MRI using gradient echos at 1.5 T. NMR Biomed 1994;7:83–99.
12. Glover GH, Lemieux SK, Drangova M, Pauly JM. Decomposition of inflow and blood oxygen level-dependent (BOLD) effects with dual-echo spiral gradient-recalled echo (GRE) fMRI. Magn Reson Med 1996;35:299–308.
13. Glover GH. Simple analytic spiral k-space algorithm. Magn Reson Med 1999;42:412–415.
14. Meyer CH, Hu BS, Nishimura DG, Macovski A. Fast spiral coronary artery imaging. Magn Reson Med 1992;28:202–213.
15. Breger RK, Rimm AA, Fischer ME, Papke RA, Haughton VH. T1 and T2 measurements on a 1.5 T commercial MR imager. Radiology 1989;171:273–276.
16. Fischer HW, Haverbeke YV, Schmitz-Feuerhake I, Muller RN. The uncommon longitudinal relaxation dispersion of human brain matter. Magn Reson Med 1989;9:441–446.
17. Wansapura JP, Holland SK, Dunn RS, Ball WS. NMR relaxation times in the human brain at 3.0 T. J Magn Reson Imag 1999;9:531–538.
18. Jezzard P, Duewell S, Balaban RS. MR relaxation times in human brain: measurement at 4 T. Radiology 1996;201:637–648.
19. Glover GH, Lai S. Self-navigated spiral fMRI: interleaved versus single-shot. Magn Reson Med 1998;39:361–368.
20. Bottomley PA, Foster TH, Argsersinger RE, Pfeifer LM. A review of normal tissue hydrogen NMR relaxation times and relaxation mechanisms from 1-100 mHz: dependence on tissue type, NMR frequency, temperature, species, excision, and age. Med Phys 1984;11:425–448.
21. Riederer SJ, Farzaneh F, Pelc NJ. Analysis of T2 limitations and off-resonance effects on spatial resolution and artifacts in echo-planar imaging. Magn Reson Med 1990;14:123–139.
22. Menon RS, Ogawa S, Tank DW, Ugurbil K. 4 Tesla gradient recalled echo characteristics of photic stimulation-induced signal changes in the human primary visual cortex. Magn Reson Med 1993;30:380–386.
23. Cohen MS, DuBois RM. Stability, repeatability, and the expression of signal magnitude in functional magnetic resonance imaging. J Magn Reson Imag 1999;10:33–40.
24. Krüger G, Fransson P, Merboldt K-D, Frahm J. Does stimulus quality affect the physiologic MRI responses to brief visual activation? NeuroReport 1999;10:1277–1281.
25. Krüger G, Frahm J, Kleinschmidt A. The cerebral blood oxygenation response to functional challenge: differences between human motor and visual cortex. Proc ISMRM 1996;3:1757.
26. Buxton RB, Wong EC, Frank LR. Dynamics of blood flow and oxygenation changes during brain activation: the ballon model. Magn Reson Med 1998;39:855–864.
27. Krüger G, Kastrup A, Takahashi A, Glover GH. Simultaneous monitoring of dynamic changes in cerebral blood flow and oxygenation during sustained activation of the human visual cortex. NeuroReport 1999;10:2939–2943.